Passive Scalar and Scalar Flux in Homogeneous Anisotropic Turbulence

A. BRIARD[a], T. GOMEZ[a], C. CAMBON[b]

a. ∂'Alembert, boîte 162, 4, Place Jussieu 75252 Paris Cedex 05
b. LMFA, Ecole Centrale de Lyon, Université de Lyon, France

Résumé :

Le but de ce travail est l'étude théorique et la modélisation d'un champ scalaire passif dans une turbulence homogène anisotrope à l'aide d'une fermeture EDQNM (Eddy-Damped Quasi-Normal Markovian) adaptée à un tel contexte. Cette fermeture est une extension du modèle spectral pour le champ de vitesse de V. Mons et. al. [10] à un champ scalaire passif et au flux scalaire, qui naît de l'interaction de gradients de vitesse et de scalaire. Des résultats généraux originaux de croissance et décroissance des énergies du scalaire et du flux en présence de gradients moyens sont ici présentés ainsi qu'une validation du modèle.

Abstract :

This work aims at studying both numerically and theoretically a passive scalar field in a homogeneous and anisotropic turbulent flow, thanks to an adapted EDQNM (Eddy-Damped Quasi-Normal Markovian) closure. This closure is an extension of the spectral model for the velocity field developed by V. Mons et. al. [10] to the passive scalar and scalar flux cases. The latter is created thanks to both velocity and scalar mean gradients. New general results regarding decay and growth laws of passive scalar and scalar flux energies in the presence of mean gradients are presented, along with the validation of the present model.

Mots clefs : Passive scalar, Scalar flux, Anisotropy, Shear flow, Mean scalar gradient

1 Introduction

The study of Homogeneous Anisotropic Turbulence (HAT) is of great interest for the complete understanding of real problems, such as atmospheric flows where scalar (temperature) and velocity gradients strongly interact. Velocity and temperature gradients can also be the consequence of boundary conditions (no-slip condition, adiabatic wall, ...).

Shear flows have received a particular attention [1, 2, 3, 4] so that some results are now well-known, such as the exponential growth of the kinetic energy and the return to isotropy of small scales, according to Kolmogorov local isotropy hypothesis [5]. The specific case of Homogeneous Isotropic Turbulence with a mean Scalar Gradient (HITSG) has also been widely studied, in particular by Bos [6]. However,

in his spectral model based on EDQNM closure, there were several adjustable constants for the velocity field and transfers kept isotropic for the passive scalar field.

Finally, the case of a shear flow with scalar gradient (HSTSG), or more generally, of HAT with both velocity and scalar gradients, has not been fully investigated yet, both numerically and theoretically. Important results are nevertheless reported by Bos [7], with the issues mentioned earlier, and the workable experimental results date back to Tavoularis and Corrsin [8].

These different points are the motivation for the present work, which is a first step into a complete HAT study. We aim at mapping the behavior of a passive scalar field under various kinds of anisotropy and for different Prandtl numbers, very large or very small. Here, both HITSG and HSTSG are investigated numerically with a fully consistent EDQNM model based on the pioneering work of Cambon [9]. Such a study of the scalar field, for different kinds of anisotropic flows, has never been performed so far, at least with an unique model that does not rely on adjustable constants (except the classical one of EDQNM). This spectral modelling has been the object of a previous work by Mons, Cambon and Sagaut [10] on the velocity field exclusively. This models relies on the intrinsic decomposition of the spectral Reynolds stress tensors into directional and polarization parts. The main equations of the existing model [10] for the velocity field are recalled. Then, the new extension to the passive scalar and scalar flux is presented. Finally, the code is validated in the HITSG and HSTSG frameworks and new results are presented in HITSG regarding the scalar variance and the cospectrum energy.

2 Equations of the model

In this part, the three final evolution equations of the anisotropic spectral model of Mons, Cambon and Sagaut [10] are given. The starting point is the dynamical equations for the full spectral tensor of velocity correlations $\hat{R}_{ij}$, in terms of the complete (3D) wave vector $\boldsymbol{k}$. These equations involve terms, which reflect the direct effect of the mean velocity gradients, that are linear and closed, and call into play unclosed contributions from third-order correlations. The latter deal with energy transfers and nonlinear pressure-strain correlations, and are closed by a generalized EDQNM procedure, as a nonlinear contribution. In the final step, the model does not retain the full spectral information, but only an optimal set of spherical-averaged descriptors, which depend on the wave vector modulus k only. This set is extracted from the decomposition of the spectral tensor $\hat{R}_{ij}$ in terms of angular spherical harmonics at the first non-trivial degree (second degree here). The evolution of the velocity field is thus driven by three sets of equations : the isotropic part of the kinetic spectrum E, its directional anisotropy part $EH_{ij}^{(dir)}$ and its polarization anisotropy part $EH_{ij}^{(pol)}$:

$$(\partial_t + 2\nu k^2)E(k,t) = S^{L(iso)}(k,t) + S^{NL(iso)}(k,t), \tag{1}$$

$$(\partial_t + 2\nu k^2)E(k,t)H_{ij}^{(dir)}(k,t) = S_{ij}^{L(dir)}(k,t) + S_{ij}^{NL(dir)}(k,t), \tag{2}$$

$$(\partial_t + 2\nu k^2)E(k,t)H_{ij}^{(pol)}(k,t) = S_{ij}^{L(pol)}(k,t) + S_{ij}^{NL(pol)}(k,t). \tag{3}$$

ν is the kinematic viscosity, $S^{NL(iso)}$, $S_{ij}^{NL(dir)}$ and $S_{ij}^{NL(pol)}$ are non-linear transfer terms fully computed with EDQNM, and $S^{L(iso)}$, $S_{ij}^{L(dir)}$ and $S_{ij}^{L(pol)}$ are linear ones, directly depending on the velocity gradients. $H_{ij}^{(dir)}$ and $H_{ij}^{(pol)}$ are deviatoric anisotropy indicators tensors linked to the spectral Reynolds

stress tensor $\hat{R}_{ij}$ through

$$2E(k,t)H_{ij}^{()}(k,t) = \int_{S_k} \hat{R}_{ij}^{()}(\boldsymbol{k},t)d^2\boldsymbol{k}, \tag{4}$$

where S_k denotes a sphere of radius k. The original result here is the extension to the passive scalar and scalax flux cases with the same compact shape. Similar calculations give the evolution of the isotropic part of the scalar spectrum E_T and its pseudo-directional part $E_T H_{ij}^{(T)}$:

$$(\partial_t + 2ak^2)E_T(k,t) = S^{T,NL(iso)}(k,t) + S^{T,L(iso)}(k,t), \tag{5}$$

$$(\partial_t + 2ak^2)E_T(k,t)H_{ij}^{(T)}(k,t) = S_{ij}^{T,NL(dir)}(k,t) + S_{ij}^{T,L(dir)}(k,t). \tag{6}$$

a is the scalar diffusivity and $H_{ij}^{(T)}$ is a pseudo scalar directional anisotropy indicator obtained with

$$2E_T(k,t)H_{ij}^{(T)}(k,t) = \int_{S_k} \mathcal{E}^{(T,dir)}(\boldsymbol{k},t)d^2\boldsymbol{k}, \tag{7}$$

where $\mathcal{E}^{(T,dir)}$ is the directional part of the spectral scalar-scalar correlation

$$< \hat{\theta}(-\boldsymbol{p})\hat{\theta}(\boldsymbol{k}) >= \mathcal{E}^T(\boldsymbol{k})\delta(\boldsymbol{k}-\boldsymbol{p}). \tag{8}$$

The scalar spectrum is simply the spherical average of $\mathcal{E}^T$, similar to $\mathcal{E}$ for the velocity field [10]. The scalar flux $F_i(\boldsymbol{k})$, or the spectral velocity-scalar cross-correlation, is driven only by one equation, as this quantity remains zero in isotropic turbulence. We define the spherical average of the scalar flux

$$E_F H_i^{(F)}(k,t) = \int_{S_k} F_i(\boldsymbol{k},t)d^2\boldsymbol{k}, \tag{9}$$

so that

$$(\partial_t + (a+\nu)k^2)E_F H_i^{(F)}(k,t) = S_i^{F,NL}(k,t) + S_i^{F,L}(k,t). \tag{10}$$

The spectrum E_F cannot exist on its own and is always linked to the anisotropy indicator $H_i^{(F)}$ as the scalar flux is zero in the isotropic framework. $S^{T,NL(iso)}$, $S_{ij}^{T,NL(dir)}$, $S_i^{F,NL}(k,t)$, $S^{T,L(iso)}$, $S_{ij}^{T,L(dir)}$ and $S_i^{F,L}(k,t)$ are the non-linear and linear passive scalar and scalar flux transfers.

For the numerical integration of these 20 independent equations, a logarithmic discretization in wave numbers is used. The kinetic and scalar spectra are initially isotropic and the scalar flux is zero. Re_λ is the Reynolds number based on Taylor microscale, and in what follows, the Prandtl number is 1, so that $\nu = a$.

3 Numerical results

3.1 Validation in HITSG

Firstly, the code is validated in the HITSG framework : the velocity field is isotropic and decays according to Comte-Bellot and Corrsin (CBC) theory [11] whereas the mean scalar gradient Λ creates the cospectrum $\mathcal{F} = E_F H_3^{(F)}$, the only non-zero component of the scalar flux, and produces scalar energy $K_T(t) = \int_0^\infty E_T(k,t)dk$. The cospectrum energy evolves as

$$\frac{dK_\mathcal{F}}{dt} = P_\mathcal{F}(t) - \epsilon_\mathcal{F}(t) + \Pi_\mathcal{F}(t) \tag{11}$$

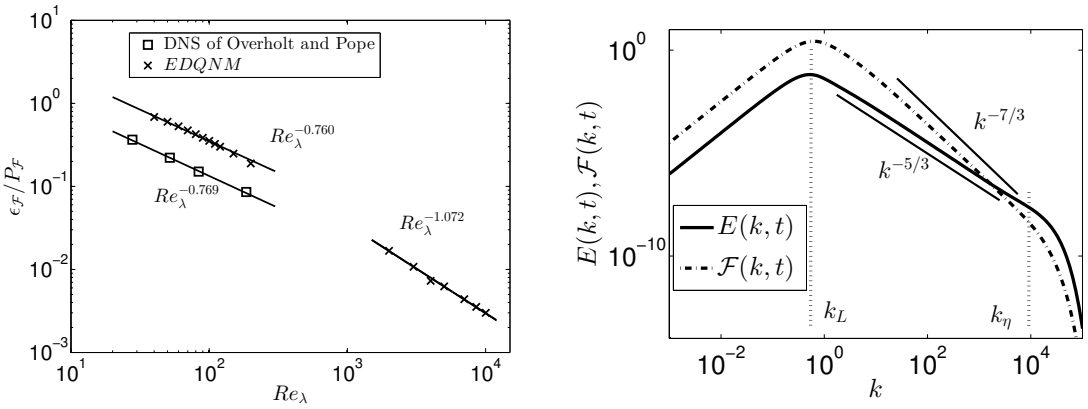

FIGURE 1 – At left, comparison of the cospectrum dissipation and production ratio with DNS. At right, the $k^{-7/3}$ range of the cospectrum $\mathcal{F}$.

where $\Pi_\mathcal{F}(t) = \int_0^\infty S_3^{F,NL}(k,t)dk$ is the cospectrum destruction, driven by pressure effects, $\epsilon_\mathcal{F}(t)$ the cospectrum dissipation rate, and $P_\mathcal{F}(t) = \int_0^\infty S_3^{F,L}(k,t)dk = \frac{2}{3}\Lambda K(t)$ the cospectrum production. The ratio of cospectrum dissipation and production is investigated and compared to the direct numerical simulation (DNS) of Overholt and Pope [12]. The initial Reynolds number is $Re_\lambda(0) = 2330$ so that inertial ranges can be clearly observed. Results are presented in Fig. 1 along with the $k^{-7/3}$ range of the cospectrum, predicted by dimensional analysis by Lumley [13]. Moreover, the theoretical Re_λ^{-1} dependence at high Reynolds number, found by Bos, is recovered as well, using a simple calculation

$$\frac{\epsilon_\mathcal{F}(t)}{P_\mathcal{F}(t)} = \frac{3(\nu+a)}{2\Lambda}\frac{\int_0^\infty k^2\mathcal{F}(k,t)dk}{\int_0^\infty E(k,t)dk} \sim \frac{\int_{k_L}^{k_\eta}\epsilon^{1/3}k^{-1/3}dk}{\int_{k_L}^{k_\eta}\epsilon^{2/3}k^{-5/3}dk} \sim Re_\lambda^{-1}$$

where $1/k_L$ is the integral scale and k_η the Kolmogorov wavenumber. The good agreement between theory, DNS and EDQNM simulations validates our code.

3.2 Decay and growth laws in HITSG

In this section, new results regarding the decay of the cospectrum in the HITSG framework are presented. The emphasis is put on the decay of the cospectrum energy

$$K_\mathcal{F}(t) = \int_0^\infty \mathcal{F}(k,t)dk.$$

We propose theoretical decay exponents, following [11], Meldi and Sagaut [14] in the isotropic case, and Briard, Gomez and Sagaut [15] for the passive scalar.

Let's introduce the infrared exponent σ so that $E(k \to 0, t) \sim k^\sigma$ and the decay exponent α of the kinetic energy $K(t) = \int_0^\infty E(k,t)dk \sim t^\alpha$. Simulations show that the cospectrum infrared slope is exactly σ and does not depend at all on the scalar one σ_T. In the high Reynolds numbers regime ($Re_\lambda \geq 200$), inertial effects are dominant and thus $K_\mathcal{F}(t) = \int_{k_L}^\infty \mathcal{F}(k,t) \sim k_L^{-4/3}\epsilon^{1/3}$. Using the well-known decay exponent of the integral scale $1/k_L$, one finds

$$K_\mathcal{F}(t) \sim t^{\alpha_\mathcal{F}}, \qquad \alpha_\mathcal{F} = -\frac{\sigma - p_\mathcal{F} - 1}{\sigma - p + 3} \tag{12}$$

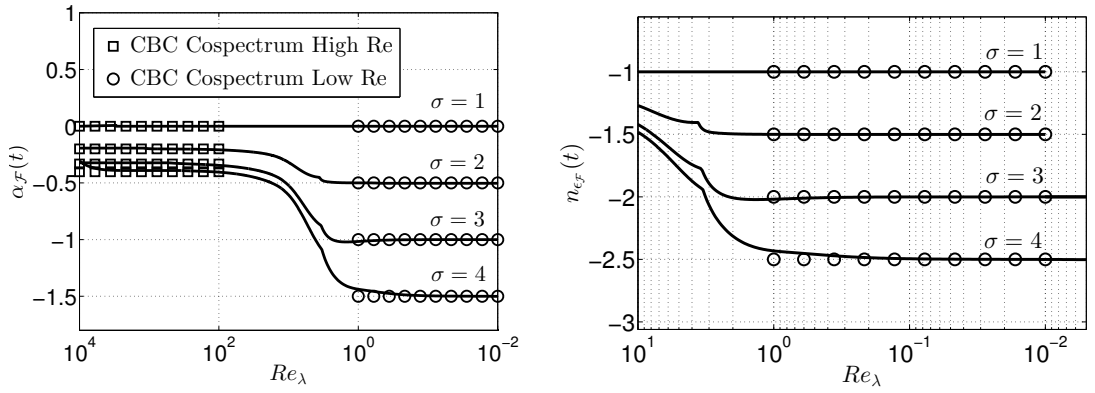

FIGURE 2 – At left, decay exponent $\alpha_{\mathcal{F}}$ of the cospectrum energy in high and low Reynolds numbers regimes for various infrared exponents σ, and at right, decay exponent $n_{\epsilon_{\mathcal{F}}}$ of the cospectrum dissipation in low Reynolds numbers regime.

where $p_{\mathcal{F}}$ is chosen to be $(p + p_T)/2$ and accounts for backscatter in Batchelor turbulence ($\sigma = 4$) and is zero otherwise. In the low Reynolds numbers regime, there are no longer inertial ranges. Hence, production effects lead the decay of the cospectrum so that $\frac{dK_{\mathcal{F}}}{dt} \sim P_{\mathcal{F}}(t)$ which directly gives

$$K_{\mathcal{F}}(t) \sim t^{\alpha_{\mathcal{F}}}, \qquad \alpha_{\mathcal{F}} = -\frac{\sigma - 1}{2}. \tag{13}$$

The great agreement between these theoretical decay exponents and numerical simulations is illustrated in Fig. 2 and is one of the main result of this paper. It is worth noting that these new results could not be obtained in existing DNS as the kinetic field was forced so that no decay could occur. As for the cospectrum dissipation $\epsilon_{\mathcal{F}}$, it is not a conserved quantity in the inertial range unlike the kinetic and scalar ones ϵ and ϵ_T. Hence, it is impossible to derive a similar power law in high Reynolds numbers regime. Nevertheless, in low Reynolds numbers regime, as inertial ranges disappear, it is possible to express the decay exponent of $\epsilon_{\mathcal{F}}$, simply as $n_{\epsilon_{\mathcal{F}}} = \alpha_{\mathcal{F}} - 1$ according to (12). This is confirmed in Fig. 2 as well.

A similar result is now presented regarding the passive scalar itself. In the presence of a mean-gradient, there is a continuous production of scalar energy according to

$$\frac{dK_T}{dt} = 2\Lambda K_{\mathcal{F}}(t) - \epsilon_T(t), \tag{14}$$

where $\epsilon_T(t)$ is the scalar energy dissipation rate. Instead of decaying [15], the scalar energy K_T grows both in high and low Reynolds numbers regimes, and scales as $\Lambda K_{\mathcal{F}}$. Using the previous results on the cospectrum exponent $\alpha_{\mathcal{F}}$, we find the scalar growth exponent α_T^{Λ} in high Reynolds numbers regime

$$K_T(t) \sim t^{\alpha_T^{\Lambda}}, \qquad \alpha_T^{\Lambda} = \frac{1}{2}\frac{p_{\mathcal{F}} - p + 8}{\sigma - p + 3} \tag{15}$$

and in low Reynolds numbers regime

$$K_T(t) \sim t^{\alpha_T^{\Lambda}}, \qquad \alpha_T^{\Lambda} = -\frac{\sigma - 3}{2}. \tag{16}$$

The good agreement between these theoretical exponents and numerical simulations is revealed in Fig.

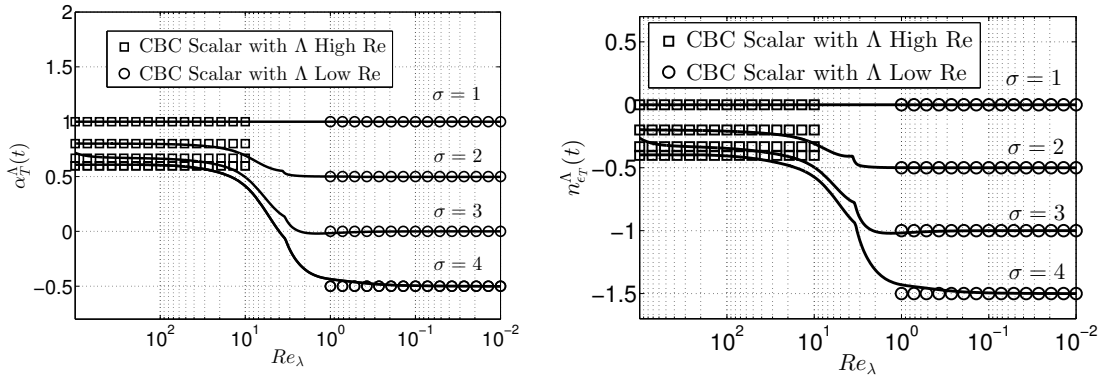

FIGURE 3 – At left, decay exponent α_T^Λ of the scalar energy in high and low Reynolds numbers regimes for various infrared exponents σ, and at right the decay exponent $n_{\epsilon_T}^\Lambda$ of the scalar dissipation rate.

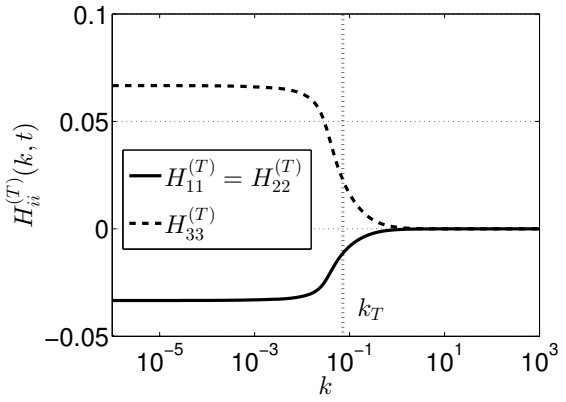

FIGURE 4 – Scalar anisotropy tensor $H_{ii}^{(T)}$ at $Re_\lambda = 200$.

3. It is interesting to point out that the growth exponent of the scalar energy with a mean gradient was already found by Chasnov [16] in the particular case of Saffman turbulence ($\sigma = 2$) where $\alpha_T^\Lambda = 4/5$. Chasnov computed analytically decay and growth exponents for passive and active scalar fields for constant and non-constant mean gradients in Saffman turbulence. His results for the active scalar were assessed by Large Eddy Simulation (LES). Our result here for the passive scalar is more general as it is valid for all kind of initial turbulence state, and can be seen as an *a posteriori* validation of Chasnov's result. The last point to explore is the behavior of the scalar dissipation rate ϵ_T which was not studied in [16]. From the evolution equation of K_T (16), it seems clear that ϵ_T behaves like $K_\mathcal{F}$ and so one simply has $n_{\epsilon_T}^\Lambda = \alpha_\mathcal{F}$, which is also recovered in Fig. 3.

A striking result is that with a mean scalar gradient, decay and growth exponents, both in high and low Reynolds numbers regimes, for the cospectrum and the scalar field, do not depend at all on the infrared scalar slope σ_T, meaning that the kinetic field fully leads the dynamics of the flow through the mean gradient Λ.

We conclude this part with a remark on the return to isotropy mechanism of small scales. Scalar anisotropy tensors $H_{ii}^{(T)}$ are displayed in Fig. 4 : they clearly show that small scales of the flow have returned to isotropy as $H_{ii}^{(T)} \to 0$ there. This is in agreement with Kolmogorov local isotropy hypothesis [5] for second-order moments.

3.3 Shear flow and scalar gradient

Here, the case of shear flow is addressed. Few results only exist regarding the passive scalar and scalar flux in presence of both velocity and scalar gradients. The shear rate is $S = dU_1/dx_3$ where U_i is the mean velocity field. Scalar indicators analogous to kinetic ones are now defined. First, the scalar shear rapidity as

$$S_R^T = \frac{\epsilon_T}{K_T S},$$

and the scalar anisotropy tensors

$$b_{ij}^T(t) = \frac{1}{K_T(t)} \int_0^\infty E_T(k,t) H_{ij}^{(T)}(k,t) dk.$$

In Fig. 5, the case of a shear flow without mean scalar gradient is presented. In such a framework, there is no scalar flux. Simulations show that S_R^T and b_{ij}^T reach constant values for $St \geq 30$, as for the analogous kinetic anisotropy indicators [4, 10].

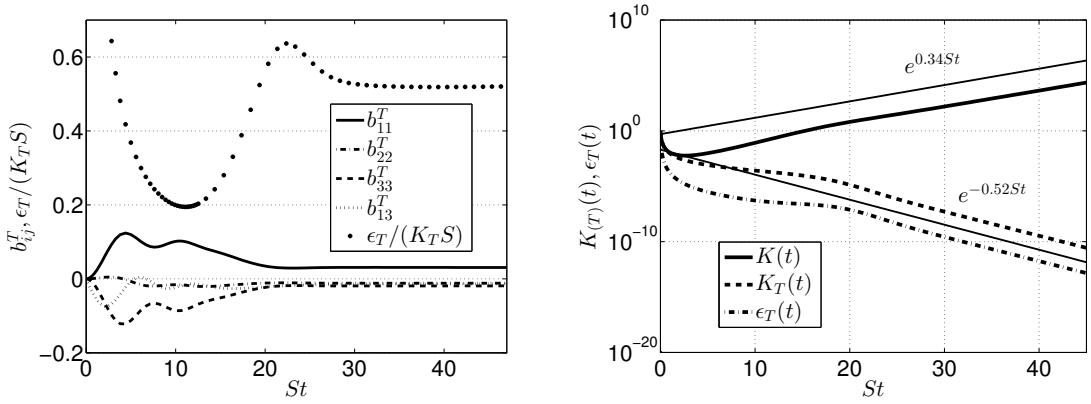

FIGURE 5 – At left, scalar anisotropy tensors b_{ij}^T with S_R^T. At right, $K(t)$, $K_T(t)$ and ϵ_T. Both for $\sigma = 2$, $\Lambda = 0$ and $S = 10^{-2}$.

Moreover, an exponential decrease of the scalar energy is observed, in agreement with the evolution equation $\partial_t K_T = -\epsilon_T$. Let's replace K_T and ϵ_T in this equation by $K_T(t) = K_T^\infty \exp(\gamma_T St)$ and $\epsilon_T(t) = \epsilon_T^\infty \exp(\gamma_T St)$. An analytical expression for the scalar exponential rate γ_T is then obtained

$$\gamma_T = -\frac{\epsilon_T}{S K_T} = -S_R^T, \qquad K_T(t) \sim K_T(0) \exp(\gamma_T St). \tag{17}$$

Such an expression for γ_T has already been obtained with different arguments by Gonzalez [17]. The exponent γ_T found by plotting K_T is in very good agreement with the asymptotic value of S_R^T, which gives $\gamma_T \simeq -0.52$. The important result is that the final value of the scalar decay rate γ_T does not depend on the shear rate S nor on the infrared exponents σ and σ_T.

When a scalar gradient is added, the scalar flux has two non-zero components. The second one, the streamwise flux $\mathcal{F}_S$, arises from shear effects, and its energy is $K_{\mathcal{F}}^S(t)$.

A short validation is proposed against Tavoularis and Corrsin [8] results in Fig. 6. Appropriate characteristic parameters give the dimensionless shear $S = 6,19$ and scalar gradient $\Lambda = 0.1823$. Let's mention that we start from an initial isotropic condition, which is clearly not the case in the experiment. Two final Reynolds numbers are given in [8] : $R_{\lambda_g} = 160$ scaled for an isotropic framework, and

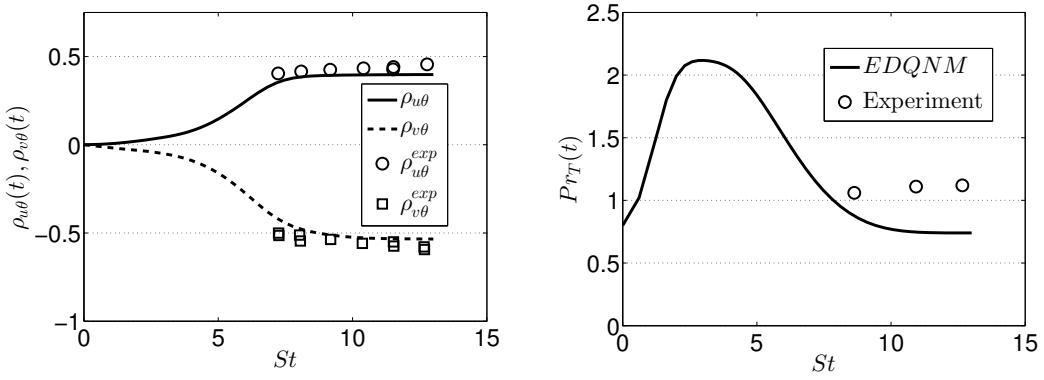

FIGURE 6 – Comparisons with experimental results of Tavoularis and Corrsin, with $\sigma = 2$, $S = 6.19$ and $\Lambda = 0.1823$.

$R_{\lambda_{11}} = 266$ for inhomogeneous flows, more appropriate. We chose the second one. Data is available at three locations : $x_1/h = 7.5$, 9.5 and 11. Using the appropriate conversion in dimensionless time this provides experimental information at $St = 8.63$, 10.94 and 12.66. There are good agreements in Fig. 6 for the cospectrum and streamwise flux correlations $\rho_{v\theta}$ and $\rho_{u\theta}$. Finally, a difference is observed for the turbulent Prandtl number

$$Pr_T(t) = \frac{\Lambda}{S}\frac{R_{12}(t)}{K_{\mathcal{F}}(t)}, \tag{18}$$

which is $Pr_T^{exp} \simeq 1.1$, whereas $Pr_T^{EDQNM} \simeq 0.74$. The value obtained experimentally seems quite large : indeed, Herring et. al. [18] and Lesieur [19] have both reported, from atmospheric data and theoretical considerations, that one should obtain $0.6 \leq Pr_T \leq 0.8$, in agreement with our result. Moreover, other values of the turbulent Prandtl numbers reported from DNS and experiments agree better with 0.7 than with 1.1. This brief comparison validates our model for the HSTSG case.

In Fig. 7, the scalar energy grows exponentially with the presence of the scalar gradient, with the same growth rate as the kinetic energy, and so do the energies of the scalar flux. This is an original result, although it could have been deduced from experimental works and existing DNS as $\rho_{v\theta}$ and $\rho_{u\theta}$ become always constant for sufficiently high St. One can see in Fig. 7 that the ratios $\epsilon_{\mathcal{F}}/(K_{\mathcal{F}}S)$ and $\epsilon_{\mathcal{F}}^S/(K_{\mathcal{F}}^S S)$ both tend to zero. This will be used in an upcoming work to give analytical expressions for the scalar flux growth rates.

4 Conclusions

This work is a step further into the theoretical and numerical study of the Homogeneous Anisotropic Turbulence. The present EDQNM spectral model relies on six equations, that can be seen as generalized Lin equations, including three for the velocity field (equations (1), (2), and (3)) which are part of the Mons, Cambon and Sagaut model [10]. The present study extends this model to the cases of a passive scalar field (equations (5) and (6)) and the associated scalar flux (equation (10)).

The model is assessed both in the frameworks of Homogeneous Isotropic Turbulence with Scalar Gradient and of Homogeneous Shear Turbulence with Scalar Gradient. New decay laws are found for the cospectrum energy $K_{\mathcal{F}}(t)$:

– In high Reynolds numbers regime, the decay is driven by inertial effects and the decrease of the kinetic energy $K(t)$.

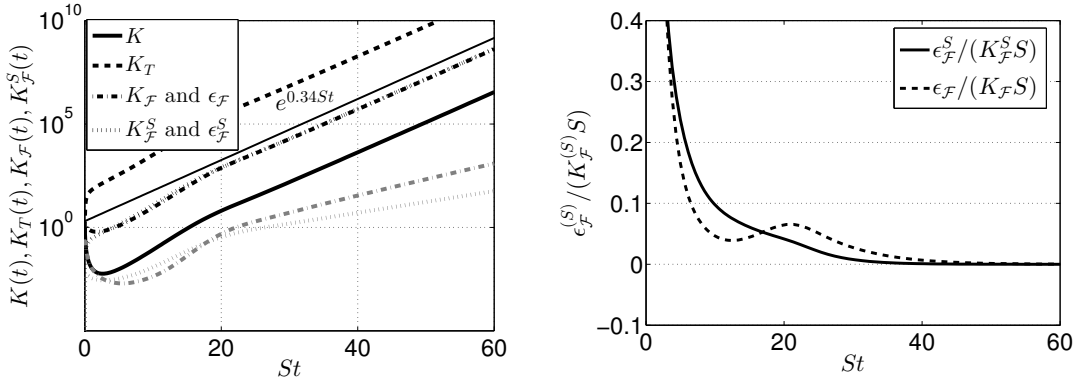

FIGURE 7 – At left, exponential growth of the kinetic, scalar, cospectrum and streamwise flux energies. The cospectrum and streamwise flux dissipation rates $\epsilon_\mathcal{F}$ and $\epsilon^S_\mathcal{F}$ are displayed in grey. At right, ratios $\epsilon_\mathcal{F}/(K_\mathcal{F}S)$ and $\epsilon^S_\mathcal{F}/(K^S_\mathcal{F}S)$. Both for $\sigma = 2$, $\Lambda = 1$ and $S = 10^{-2}$.

– In the low Reynolds numbers regime, as inertial effects are negligible, production of cospectrum leads the decay.

The decay exponent of the cospectrum dissipation rate $\epsilon_\mathcal{F}(t)$ is found as well, only in the low Reynolds numbers regime, in agreement with Bos study [6]. Similarly, the scalar dissipation rate $\epsilon_T(t)$ is found to decay as $K_\mathcal{F}(t)$, whereas the scalar energy $K_T(t)$ grows with time because of the production term linked to the cospectrum. The latter is in agreement with the theoretical work of Chasnov [16] in Saffman turbulence, and thus can be seen as a generalization and an additional validation.

The strong result with these new theoretical exponents, assessed with numerical simulations, is that they do not depend on the intensity of the scalar gradient Λ, nor on the scalar large scales initial conditions σ_T ($E_T(k \to 0, t) \sim k^{\sigma_T}$). Therefore, we conclude that in HITSG, the passive scalar is fully dominated by the velocity field, even its large scales.

Then, the cases of a passive scalar with shear only, and shear combined with scalar gradient, are briefly investigated. In the first case, the exponential decrease of the scalar energy $K_T(t)$ is recovered both numerically and analytically. In the second case, all energies are found to grow exponentially with the same rate γ as the kinetic field, found in [10]. These two last cases deserve more investigation and are at the center of an upcoming work, along with the influence of a Prandtl number very different from 1.

Références

[1] S. Tavoularis, U. Karnik, *Further experiments on the evolution of turbulent stresses and scales in uniformly sheared turbulence*. J. Fluid Mech. (204), 1989.

[2] A. Pumir, B. I. Shraiman, *Persistent Small Scale Anisotropy in Homogeneous shear flows*. Phys. Rev. Lett. (75), 1995.

[3] F. A. De Souza, V. D. Nguyen, S. Tavoularis, *The structure of highly sheared turbulence*. J. Fluid Mech. (303), 1995.

[4] P. Sagaut, C. Cambon, *Homogeneous Turbulence Dynamics*. Cambridge University Press, 2008.

[5] A. N. Kolmogorov, *The local structure of turbulence in incompressible viscous fluid for very large Reynolds numbers*. Dokl. Akad. Nauk SSSR (30), 1941.

[6] W. J. T. Bos, H. Touil, J.P. Bertoglio, *Reynolds number dependency of the scalar flux spectrum in isotropic turbulence with a uniform scalar gradient*. Phys. Fluids (17), 2005.

[7] W. J. T. Bos, J.P. Bertoglio, *Inertial range scaling of scalar flux spectra in uniformly sheared turbulence*. Phys. Fluids (19), 2007.

[8] S. Tavoularis, S. Corrsin, *Experiments in nearly homogenous turbulent shear flow with a uniform mean temperature gradient. Part 1*. J. Fluid Mech. (104), 1981.

[9] C. Cambon, D. Jeandel, J. Mathieu, *Spectral modelling of homogeneous non-isotropic turbulence* . J. Fluid Mech. (104), 1981.

[10] V. Mons, C. Cambon, P. Sagaut, *A new spectral model for homogeneous anisotropic turbulence with application to shear-driven flows and return to isotropy* . J. Fluid Mech. (Submitted), 2015.

[11] G. Comte-Bellot, S. Corrsin, *The use of a contraction to improve the isotropy of grid-generated turbulence*. J. Fluid Mech. (25), 1966.

[12] M. R. Overholt, S. B. Pope, *Direct numerical simulation of a passive scalar with imposed mean gradient in isotropic turbulence*. Phys. Fluids (8), 1996.

[13] J. L. Lumley, *Similarity and the Turbulent Energy Spectrum*. Phys. Fluids (10), 1966.

[14] M. Meldi, P. Sagaut, D. Lucor, *A stochastic view of isotropic turbulence decay*. J. Fluid Mech. (668), 2011.

[15] A. Briard, T. Gomez, P. Sagaut, S. Memari *Passive scalar decay laws in isotropic turbulence : Prandtl effects*. J. Fluid Mech. (Reviewed), 2015.

[16] J. R. Chasnov, *Similarity states of turbulence passive scalar transport in buoyancy-generated*. Phys. Fluids (7), 1995.

[17] M. Gonzalez, *Asymptotic evolution of a passive scalar advected by homogeneous turbulent shear flow*. Int. J. Heat Mass Tran. (43), 2000.

[18] J. R. Herring, et. al., *A comparative assessment of spectral closures as applied to passive scalar diffusion*. J. Fluid Mech. (124), 1982.

[19] M. Lesieur, *Turbulence in Fluids*. Springer, 4th Edition, 2008.